L-Edge X-ray magnetic circular dichroism of Ni enzymes: direct probe of Ni spin states

Hongxin Wang[a,b], Daulat S. Patil[b], Corie Y. Ralston[a], Craig Bryant[a],
Stephen P. Cramer[a,b,*]

[a]*Department of Applied Science, University of California, Davis, CA 95616, USA*
[b]*Lawrence Berkeley National Laboratory, Berkeley, CA 94720, USA*

Abstract

X-ray magnetic circular dichroism (XMCD) measures the inner shell absorption difference between left and right circularly polarized X-rays in the presence of magnetic field, and provides us a direct probe of the spin values localized in the specific metal sites. In this study, using *Desulfovibrio desulfuricans* and *Desulfovibrio gigas* hydrogenases as examples, we have measured the L-edge XMCD of Ni enzymes for the first time and analyzed them in comparison with a doped high spin Ni^{II} model complex. The reduced hydrogenases have a non-zero XMCD effect, which is consistent with a 'high spin' Ni^{II} site. The magneto-optical sum rules have also been used to derive the orbital and spin angular momentum. © 2001 Elsevier Science B.V. All rights reserved.

Keywords: Ni enzymes; Hydrogenase; Magnetic circular dichroism; Circular polarization; XMCD; Sum rules

1. Introduction

The variety of nickel's oxidation states (from -1 to $+4$) and local geometry (octahedral, tetrahedral, tetragonal, trigonal bi-pyramidal and square planar, etc.) make Ni complexes important in coordination chemistry. In biology, Ni is an essential trace element in a large variety of enzymes, such as Ni–Fe hydrogenase [1]. Ni–Fe hydrogenase, which catalyzes the oxidation and formation of molecular hydrogen (H_2), is one of the most important Ni enzymes. It exists in several organisms, such as

Desulfovibrio gigas, *Desulfovibrio desulfuricans*, *Desulfovibrio baculatus* and *Pyrococcus furiosus* [1]. Although different in protein structures, all of these hydrogenases have similar functional metal sites: one Ni–Fe center for catalysis and two or three Fe–S clusters for electron transfer [2,3]. As reported previously, for *D. gigas* hydrogenase, the Ni is basically covalent Ni^{III} in as-isolated Ni–A state but can be Ni^0, Ni^I or Ni^{II} in H_2 reduced Ni–R form according to different proposals [4–6]. Another important issue concerning the nickel's electronic configuration in Ni–Fe hydrogenases is its unclear spin state in the H_2 reduced form. A Ni^{II} configuration has eight electrons in five 3d orbitals. A high spin Ni^{II} has two unpaired electrons while the other six electrons paired, leading to S=1. In contrast, a

low spin Ni^{II} has all the eight electrons paired, yielding S=0. Although most of the previous studies assign Ni–R to low spin Ni^{II} [2,7–9], an octahedral complex with two hydride ligands or a trigonal pyramidal complex with a single hydride [10,11] would be consistent with high-spin Ni^{II}. Our recent L-edge absorption spectrum of H_2 reduced *D. gigas* hydrogenase also illustrates a clear high spin Ni^{II} multiplet [12,13].

X-ray magnetic circular dichroism (XMCD) measures the inner shell absorption difference between left and right circularly polarized X-rays in presence of magnetic field [14], and can provide a direct probe of the spin values localized in the specific metal sites. For example, there is usually no XMCD effect in a zero spin complex. With magneto-optical sum rules [14–16], it is possible to derive the metal's orbital and spin angular momentum separately. X-ray magnetic circular dichroism is element specific in contrast to traditional magnetic measurements, such as EPR spectroscopy. It also provides more information than the regular X-ray absorption spectroscopy [14]. In comparison with K-edge XMCD, L-edge XMCD has several additional advantages, including a much larger MCD effect [17].

The origin of XMCD is the consequence of the selection rules for electric dipole-allowed transitions, and the XMCD effect relies on the non-uniform occupation of the Zeeman-split levels in the initial state. The former needs a circular polarized X-ray source while the latter requires magnetization. In comparison with experiments on solid state materials [14], high magnetic fields or extremely low temperatures are required when trying to magnetize dilute and paramagnetic biological metals [17,18]. As ultrahigh magnetic field (>3 Tesla) will interfere with the performance of a X-ray fluorescence detector, extremely low temperature is usually preferred [19]. In this study, a newly constructed third-generation XMCD apparatus with a superconductor magnet (2 Tesla) and a dilution refrigerator (T=~0.5 K) has been used to magnetize Ni–Fe hydrogenase samples. The XMCD of as-isolated *D. gigas* hydrogenase and H_2 reduced *D. gigas/D. desulfuricans* hydrogenases are measured for the first time and compared with the XMCD of a high spin Ni^{II} model.

2. Experimental section

2.1. XMCD measurement

Our XMCD measurement was performed at the Stanford Synchrotron Radiation Laboratory (SSRL) bend magnet beamline 8-2 [20] using the 1100 l/mm grating. Elliptically polarized X-rays were obtained by moving the first mirror above or below the electron orbit plane (Fig. 1a) [21]. Based on previous calibration on polarized ferromagnetic samples [21] and a Ni-doped MgO crystal [22], the optimum XMCD signal was obtained at a beam take off angle
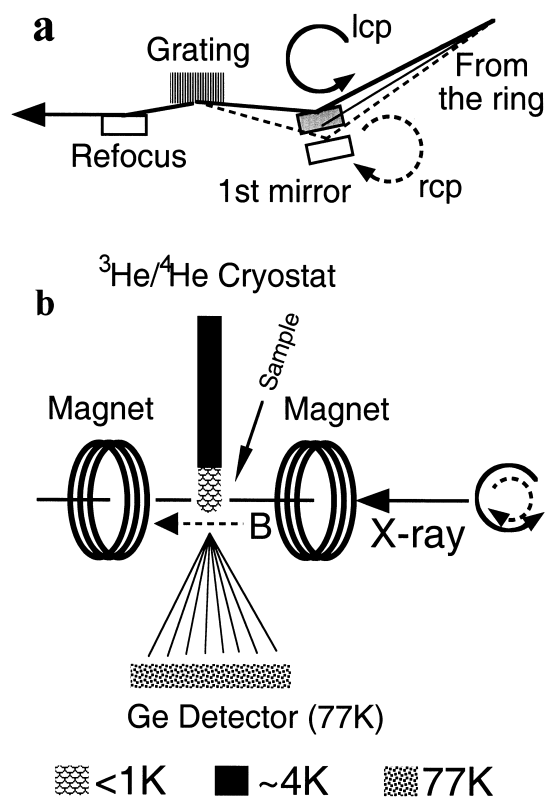

Fig. 1. The schematic diagram of our XMCD instrumentation. (a) The left/right elliptical polarized X-ray is obtained by moving the first mirror above/under the electron orbital ring in a bent magnet beamline. (b) The XMCD measurement setup. The sample is kept under <1 K with a $^3He/^4He$ dilution fridge, and is magnetized with a pair of superconducting magnets (2 Tesla). The X-ray fluorescence signal was collected with a 30-element Ge array detector and the whole apparatus is under windowless operation.

corresponding to a circular polarization of $80\pm5\%$ [18,21]. At this take off angle the beam intensity is 75% off its maximum value at the plane axis. The entrance and exit slits were both set to 60 μm, and the energy resolution was estimated to be 1.4 eV for circular polarized X-ray.The XMCD apparatus (Fig. 1b) uses a 76-cm split-coil 2 Tesla superconducting magnet (at 4 K) surrounded by a UHV chamber maintained at $\sim5\times10^{-9}$ Torr [18]. The cold finger of a ^{3}He/^{4}He dilution refrigerator enters the magnet bore from the top of the chamber and the sample is attached to the cold finger at the center of the magnet. The whole chamber is shielded with 4 K liquid helium and 77 K liquid nitrogen. The cold finger's temperature was measured with a carbon resistance thermometer (Matsushita) and confirmed by the field-dependent XMCD effects for doped model Ni^{II} complex [18]. Least-squares fitting with a Brillouin function for a $J=1$ system gives a temperature of ~0.6 K, corresponding to >99% magnetic saturation at 2 Tesla. Ni enzyme samples were measured under the same condition. A 30-element windowless Ge fluorescence detector [22] (77 K) [23] is inserted horizontally between the two coils, perpendicular to the incident X-ray photon beam. The data acquisition is as described in the preceding paper [13]. Individual scans were taken over the Ni L-edges using 0.2-eV steps at 30 s per point integration time for enzyme samples and 15 s for the doped Ni model. One set of 20 scans was taken with 'right' circular polarized X-ray. Every two scans, the magnetic field was switched between -2 and 2 Tesla. A second set of 20 scans was then measured with 'left' circular polarized X-ray, again alternating the sign of the magnetic field. As expected, the XMCD effect did reverse with opposite beam polarization or opposite magnetic field. These scans were then classified into two categories, the ones with the 3d electronic spin being parallel to the X-ray helicity ($I^{\uparrow\uparrow}$) and the ones with the 3d spin being antiparallel ($I^{\uparrow\downarrow}$) to the X-ray helicity [18]. The final spectrum is the sum of 20 individual scans for each side.

2.2. XMCD analysis

Each side of the averaged spectra was first corrected for the small energy offset between spectra

recorded on opposite polarization [18,21]. A cubic polynomial was then fit to the raw data in the pre-L_3 and post-L_2 regions to simulate the two-step non-resonant (background) X-ray absorption. The nonresonant steps were then subtracted from the overall spectrum, leaving only the resonant component of the absorption signal. Finally the spectra were corrected for the fact that the illuminating X-rays were only 80% polarized, by [18]

$$I^{\uparrow\uparrow} = \{(\alpha+1)\cdot I_m^{\uparrow\uparrow} + (\alpha-1)\cdot I_m^{\uparrow\downarrow}\}/2\alpha \qquad (1)$$

$$I^{\uparrow\downarrow} = \{(\alpha+1)\cdot I_m^{\uparrow\downarrow} + (\alpha-1)\cdot I_m^{\uparrow\uparrow}\}/2\alpha \qquad (2)$$

$$\mathrm{XMCD} = (I^{\uparrow\uparrow} - I^{\uparrow\downarrow})/(I^{\uparrow\uparrow} + I^{\uparrow\downarrow})$$
$$= \{(I_m^{\uparrow\uparrow} - I_m^{\uparrow\downarrow})/(I_m^{\uparrow\uparrow} + I_m^{\uparrow\downarrow})\}/\alpha \qquad (3)$$

where the $I_m^{\uparrow\uparrow}$ and $I_m^{\uparrow\downarrow}$ represent the observed spectra, the α is the degree of X-ray polarization, the $I^{\uparrow\uparrow}$, $I^{\uparrow\downarrow}$ and XMCD are the polarization-corrected intensities.

Two important magneto-optical sum rules [15,16,18] can be used to relate the integrated XMCD intensities to element-specific projections of the 3d orbital angular momentum $\langle L_z\rangle$, the 3d spin angular momentum $\langle S_z\rangle$, and a magnetic dipole term $\langle T_z\rangle$. In this study, the $\langle T_z\rangle$ is negligible for the highly symmetric (octahedral) Ni-doped MgO crystals [24] and is averaged to zero for Ni enzymes [14,18]. Omitting $\langle T_z\rangle$ term, approximating I^0 by $(I^{\uparrow\uparrow} + I^{\uparrow\downarrow})/2$, and using the common symbols in the XMCD literature [14,18,21], one can thus express the sum rules for 3d transition metal L-edges as (in/atom):

$$\langle \mathbf{L}_z\rangle/n_h = -2(A+B)/(3C)\langle\mathbf{S}_z\rangle/n_h$$
$$= -(A-2B)/2C \qquad (4)$$

where n_h represents the number of 3d vacancies in the metal ion, 'A' and 'B' refer to the integral of the XMCD spectrum over the L_3 and L_2 regions, respectively, and 'C' refers to the integral of the spectrum $(I^{\uparrow\uparrow} + I^{\uparrow\downarrow})/2$ over the whole L_3 and L_2 region. As covalencies of our Ni samples are unknown, orbital and spin angular momentum per unit hole are obtained and compared.

2.3. Samples preparation

The enzymes from *Desulfovibrio* bacteria grown on a sulfate–lactate medium were purified by ion-exchange chromatography and purified as reported previously [25]. The specific activity was estimated by measuring the hydrogen gas evolved in a reaction using methyl viologen as electron carrier and dithionite as reductant. The *D. gigas* hydrogenase sample was prepared in as-isolated and H_2 reduced forms, while the *D. desulfuricans* hydrogenase sample was only made in H_2 reduced form. The film samples for the L-edge XMCD measurement were prepared by syringing a drop (~20 μl) of protein solution onto a gold plated sample holder and allowing it to dry under the appropriate atmosphere. The film samples were transferred anaerobically to the measurement chamber by a loadlock. Ni-doped MgO crystal (0.14%, Goodfellow) was used as a high spin Ni^{II} model [26].

3. Results and discussion

3.1. XMCD of Ni^{II} Model

For comparison with the measured Ni enzyme XMCD, we have first examined XMCD for a known high spin Ni^{II} complex: Ni-doped MgO crystal [26]. The Ni L-edge excitation spectra of this complex for the Ni 3d electronic spin being parallel ($I^{\uparrow\uparrow}$) and antiparallel ($I^{\uparrow\downarrow}$) to the X-ray helicity are shown in Fig. 2a. The L_3 region has a major peak near 853.6 eV and a minor peak near 855.7 eV, exhibiting a typical high-spin (triplet state) Ni^{II} spectrum [24]. The L_2 at 868–873 eV has a partially resolved doublet structure, again a typical high-spin Ni^{II} feature. Although some previous reports revealed spectral distortion with fluorescence detection [27], the 'distortion' in our spectrum for this dilute (0.14%) Ni^{II} ion appears insignificant, in comparison with a total electron yield measured high spin Ni^{II} ion in $Cs[Ni^{II}Cr^{III}(CN)_6]·2H_2O$ [24].

The polarization-corrected difference in fluorescence signal ($I^{\uparrow\uparrow}-I^{\uparrow\downarrow}$) — the X-ray magnetic circular dichroism, is shown in Fig. 2b. At the L_3 edge there is a 44% difference in polarization-cor-
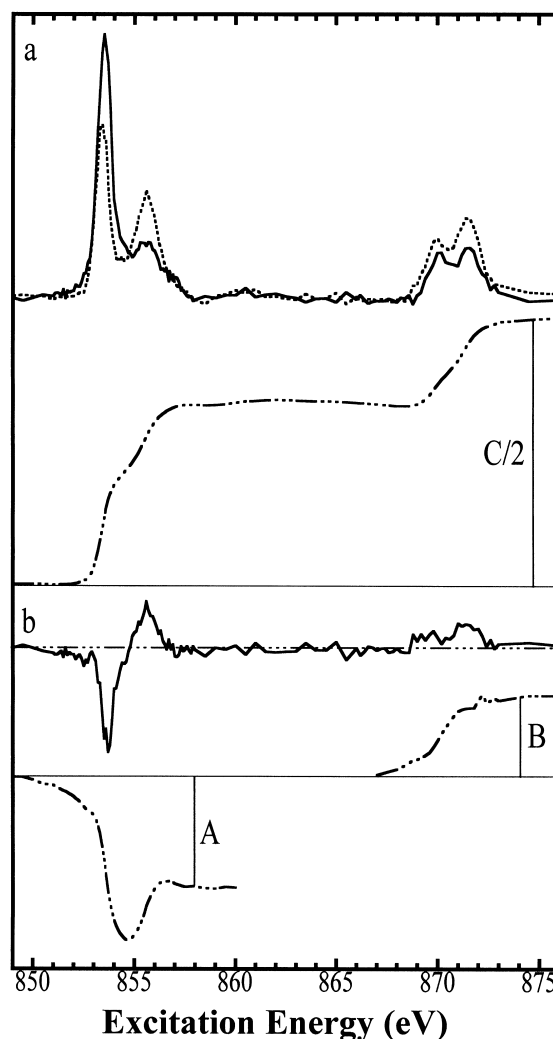

Fig. 2. (a) Polarization-normalized, background-subtracted excitation spectra for Ni doped in MgO crystal, taken with photon angular momentum in parallel (solid line) and in antiparallel (dash line) to Ni 3d electronic spin. The multiplet structure confirms a high spin Ni^{II} species. (b) Polarization-corrected XMCD spectrum for the Ni doped in MgO. The dot-dash line under the excitation spectra is one half of the integrated intensity of the spectrum of $(I^{\uparrow\uparrow}+I^{\uparrow\downarrow})/2$ over the whole L_3 and L_2 region ($C/2$) while the dot-dash lines under the difference spectrum are the integral of the XMCD spectrum over the L_3 and L_2 regions (A and B), respectively,.

rected absorption intensity between the two peaks, corresponding to 22% XMCD effect. At L_2, XMCD effect is smaller but still 20%. The two resolved peaks at the L_3 edge have opposite sign XMCD

signals (intensity ratio, 3:1), while the two at the L_2 have the same sign. The opposite XMCD sign at the L_3 is because the main L_3 peak corresponds to excitations with the final $2p^5$ spin parallel to the $3d^9$ spin, while the secondary peak is the transition with the final $2p^5$ spin antiparallel to the $3d^9$ spin. This is the nature of high spin Ni^{II} complexes [22,24], not the effect of anti-ferromagnetic interactions [28].

3.2. D. desulfuricans hydrogenase

Hydrogen reduced *D. desulfuricans* hydrogenase has similar Ni absorption and XMCD spectra (Fig. 3ab) with the above-discussed high spin Ni^{II} model complex. The L_3 has a major peak near 853.6 eV and a minor peak (for $I^{\uparrow\downarrow}$)/a shoulder (for $I^{\uparrow\uparrow}$) near 855.2 eV. The L_2 has a barely resolved doublet structure at 868–873 eV. In comparison with the Ni doped in MgO, some differences are noticed as well. At L_3, only one side ($I^{\uparrow\downarrow}$) of the absorption spectra has a secondary peak while another side only has a unresolved shoulder. The separation in between the main and secondary structures of the L_3 edge is 0.6 eV for *D. desulfuricans* hydrogenase and 1.1 eV for Ni doped MgO. The smaller separation is consistent with the more covalent Ni–S interaction in *D. desulfuricans* hydrogenase than the Ni–O interaction in Ni/MgO.

There is a 27.5% difference in polarization-corrected absorption intensity between the two spectra at L_3, corresponding to 14% XMCD effect. The XMCD signal at L_3 exhibits a bipolar multiplet, similar with Ni-doped MgO crystal. The statistical analysis using the XMCD data off the L_3 and L_2 peak regions reveals error lines of $\pm 2\sigma$ as shown in Fig. 3 (dot-dash lines). The XMCD intensity at L_3 is significant in comparison with the error bars while the XMCD at L_2 is not so obvious. Differences in between the XMCD spectrum for *D. desulfuricans* hydrogenase and that for Ni/MgO include a smaller (14 vs. 22%) XMCD effect at L_3 edge and clear differences at L_2 edge. Nevertheless the active XMCD effect and bipolar XMCD multiplet at L_3 indicates that the Ni in *D. desulfuricans* hydrogenase is high spin Ni^{II}, not low spin Ni^{II}.

For sum rule analysis, the necessary integrals *A*, *B* and *C* (dot-dash lines) are illustrated in Fig. 3. The
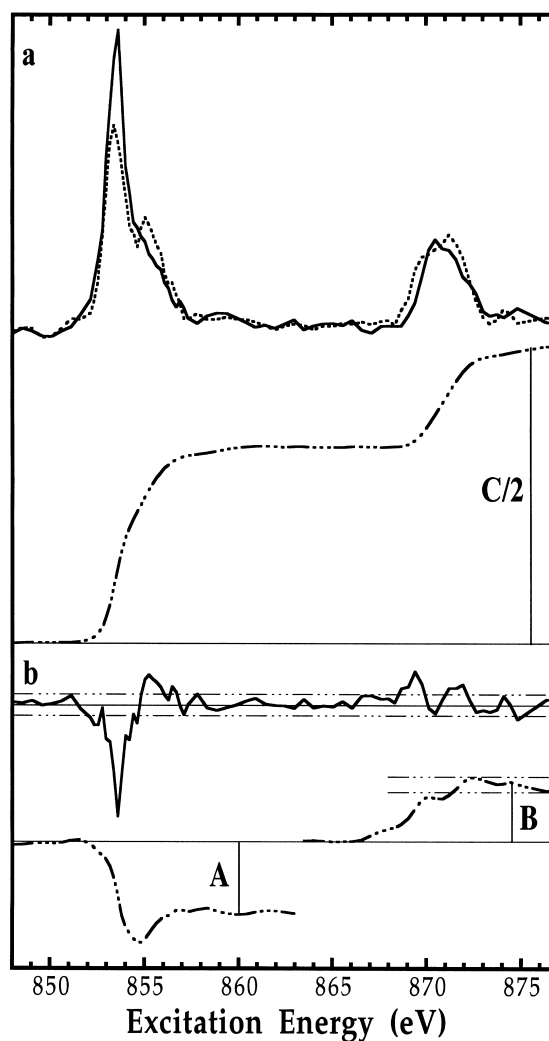

Fig. 3. (a) Polarization-normalized, background-subtracted excitation spectra for Ni in H_2 reduced *D. desulfuricans* hydrogenase, taken with photon angular momentum in parallel (solid line) or antiparallel (dash line) to Ni 3d spin. (b) Polarization-corrected XMCD spectrum for reduced *D. desulfuricans* hydrogenase. The dot-dash lines under the absorption and XMCD spectra are the integrals of *C*/2, *A* and *B*, respectively. The dot-dash lines associated with the XMCD spectra are the error lines ($\pm 2\sigma$) based on the statistics of the XMCD data off the L_3 and L_2 regions.

calculated values are $A = 3.0 \pm 0.3$, $B = 2.2 \pm 0.3$, and $C = 14.0 \pm 0.6$. Substituting $n_h = 1$ (for unit hole) into formula (4), we have found the orbital and spin angular momentum $\langle L_z \rangle / n_h$ and $\langle S_z \rangle / n_h$ to be 0.02 ± 0.02 and 0.14 ± 0.02, respectively. The error analysis is based on statistical error plus 10%

instrumental error. The large error in $\langle L_z \rangle$ is due to the large error in XMCD at L_2. For comparison, sum rule analysis on the high spin Ni^{II} model complex is also performed. The integrals *A*, *B* and *C* are illustrated in Fig. 2 (dot-dash lines), with $A = 4.5 \pm 0.3$, $B = 3.0 \pm 0.2$ and $C = 18.8 \pm 0.6$. The derived orbital and spin angular momentum (per hole)
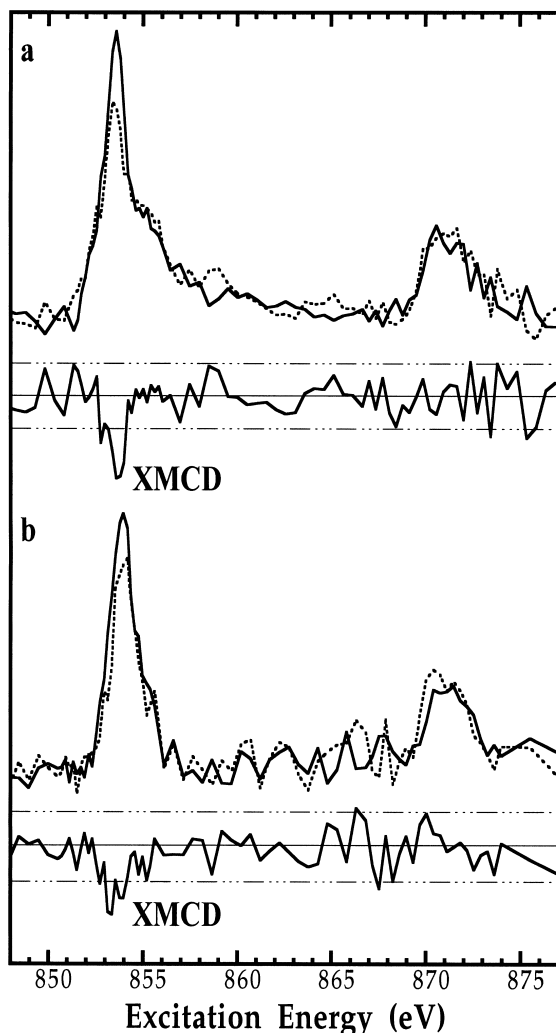

Fig. 4. Polarization-normalized, background-subtracted excitation spectra for Ni in hydrogen reduced (upper) and as-isolated (lower) *D. gigas* hydrogenase. The difference spectra under them (solid lines) are the polarization-corrected XMCD spectra. The dot-dash lines associated with the XMCD spectra are the error lines ($\pm 2\sigma$) based on the statistics of the XMCD data off the L_3 and L_2 regions.

$\langle L_z \rangle / n_h$ and $\langle S_z \rangle / n_h$ are 0.05 ± 0.02 and 0.28 ± 0.02. The difference is expected because they are from different systems.

3.3. Preliminary results of D. gigas

In the preceding paper [13], our Ni L-edge spectroscopy reveals evidence of high spin Ni^{II} in H_2 reduced *D. gigas* hydrogenase. In Fig. 4a, although the minor L_3 shoulders are not resolved, the circular polarized absorption spectra for the H_2 reduced *D. gigas* hydrogenase show similar spectral multiplet as observed in our L-edge spectra in the preceding paper as well as the circular polarized absorption spectra of Ni doped in MgO and *D. desulfuricans* hydrogenase, again illustrating a typical high spin Ni^{II} feature. The circular polarized absorption spectra for as-isolated *D. gigas* hydrogenase are shown in Fig. 4b. The spectra are similar with a covalent Ni^{III}, without any sharp multiplet [12].

Fig. 4 shows a relatively 'small' XMCD effect for both as-isolated and H_2 reduced *D. gigas* hydrogenase because the signal-to-noise ratio (S/N) is not satisfactory. The errors ($\pm 2\sigma$) in XMCD spectra are also shown in Fig. 4, based on the statistics on the XMCD data off the L_3 and L_2 regions. Although a quantitative assignment is not possible, it is still clear to see that the XMCD intensity (at L_3) for H_2 reduced *D. gigas* hydrogenase is bigger than (almost twice the size as) the error bar, exhibiting a non-zero spin for this species. A low spin Ni^{II} site should have a zero spin value and should be XMCD inactive. The as-isolated *D. gigas* hydrogenase has a XMCD that is just a little bit bigger than the statistical error bar. Better XMCD studies are necessary in the future for the *D. gigas* hydrogenase.

4. Summary

In this study, we have measured the Ni L-edge X-ray magnetic circular dichroism (XMCD) of Ni in the *D. desulfuricans* and *D. gigas* hydrogenases for the first time and analyzed them in comparison with a known high spin Ni^{II} model complex (Ni/MgO). The Ni/MgO and the H_2 reduced *D. desulfuricans* hydrogenase has a clear XMCD effect, a bipolar XMCD multiplet, which is consistent with a 'high

spin' Ni^{II} site. Two magneto-optical sum rules have also been used to derive the Ni orbital and spin angular momentum from XMCD spectra of these two Ni samples. Although no quantitative assignment has been made for the H_2 reduced *D. gigas* hydrogenase, it still exhibits a non-zero XMCD effect, consistent with a high spin Ni^{II} assignment [13].

Undulator beamlines in the third generation synchrotron radiation light sources can provide several orders of magnitude higher photon flux for up to 100% circular polarized X-rays. For instance, the magnetic spectroscopy beamline 4.0.2 in advanced light source has photon flux of 6×10^{12} photons/s per 0.1%-bandwidth at 700 eV at 400 mA ring current. In addition, rapid changing of the X-ray helicity makes it possible to record point-to-point XMCD spectra instead of several scans on one side. Our XMCD has demonstrated its usefulness in direct probe of Ni the electron spin states in Ni enzymes and illustrated a great promise for the future development of biological X-ray magnetic circular dichroism.

Acknowledgements

References

[1] J.R. Lancaster, in: The Bioinorganic Chemistry of Nickel, VCH, New York, 1988.

[2] S.P.J. Albracht, Biochim. Biophys. Acta — Bioenergetics 1188 (1994) 167–204.

[3] J.C. Fontecilla-Camps, Structure Bonding 91 (1998) 2–30.

[4] J.W. van der Zwaan, S.P.J. Albracht, R.D. Fontijn, E.C. Slater, FEBS Lett. 179 (1985) 271.

[5] R. Cammack, C. Bagyinka, K.L. Kovacs, Eur. J. Biochem. 182 (1989) 357–362.

[6] J.J.G. Moura, M. Teixeira, I. Moura, Pure Appl. Chem. 61 (1989) 915.

[7] Z.J. Gu, J. Dong, C.B. Allan, S.B. Choudhury, R. Franco, J.J.G. Moura, J. Legall, A.E. Przybyla, W. Roseboom, S.P.J. Albracht, M.J. Axley, R.A. Scott, M.J. Maroney, J. Am. Chem. Soc. 118 (1996) 11155–11165.

[8] C.P. Wang, R. Franco, J.J.G. Moura, I. Moura, E.P. Day, J. Biol. Chem. 267 (1992) 7378–7380.

[9] F. Dole, A. Fournel, V. Magro, E.C. Hatchikian, P. Bertrand, B. Guigliarelli, Biochemistry 36 (1997) 7847–7854.

[10] P. Amara, A. Volbeda, J.C. Fontecilla-Camps, M.J. Field, J. Am. Chem. Soc. 121 (1999) 4468–4477.

[11] E. Garcin, X. Vernede, E.C. Hatchikian, A. Volbeda, M. Frey, J.C. Fontecilla-Camps, Structure Folding Design 7 (1999) 557–566.

[12] H.-X. Wang, C.Y. Ralston, D.S. Patil, R.M. Jones, W.-W. Gu, S.P. Cramer, J. Am. Chem. Soc. 122 (2000) 10544–10552.

[13] H. Wang, D.S. Patil, W. Gu, L. Jacquamet, S. Friedrich, T. Funk, S.P. Cramer, J. Electron Spectrosc. 114–116 (2001) 855–863.

[14] J. Stohr, H. Kong, Phys. Rev. Lett. 75 (1995) 3748.

[15] B.T. Thole, P. Carra, F. Sette, G. van der Laan, Phys. Rev. Lett. 68 (1992) 1943–1946.

[16] P. Carra, B.T. Thole, M. Altarelli, X.D. Wang, Phys. Rev. Lett. 70 (1993) 694–697.

[17] S.P. Cramer, C.Y. Ralston, H.-X. Wang, C. Bryant, J. Electron Spectrosc. 86 (1997) 175–183.

[18] H.-X. Wang, C. Bryant, D.W. Randall, L.B. LaCroix, E.I. Solomon, M. LeGros, S.P. Cramer, J. Phys. Chem. B 102 (1998) 8347–8349.

[19] S.P. Cramer, P.G.J. Christians, J. Chen, J. van Elp, S.J. George, A.T. Young, J. Electron Spectrosc. 78 (1996) 225–229.

[20] L.J. Terminello, G.D. Waddill, J.G. Tobin, Nucl. Instrum. Methods A A319 (1992) 271–276.

[21] R. Nakajima, Ph. D. Dissertation, Stanford University 1997.

[22] C. Bryant, H.-X. Wang, M. LeGros, X. Wang, S.P. Cramer, J. Synchrotron Radiation (2000) to be submitted.

[23] S.P. Cramer, J. Chen, S.J. George, J. Vanelp, J. Moore, O. Tensch, J. Colaresi, M. Yocum, O.C. Mullins, C.T. Chen, Nucl. Instrum. Methods A 319 (1992) 285–289.

[24] M.A. Arrio, S.P. Moulin, C.C.D.C. Brouder, F.M.F. de Groot, T. Mallah, M. Verdaguer, J. Phys. Chem. 100 (1996) 4679–4684.

[25] D.S. Patil, Methods Enzymol. 243 (1994) 68–94.

[26] J.W. Orton, J.E. Wertz, Phys. Rev. Lett. 4 (1960) 128.

[27] F.M.F. de Groot, J. Electron Spectrosc. 67 (1994) 529–622.

[28] P. Rudolf, F. Sette, L.H. Tjeng, J. Magn. Magn. Mater. 109 (1992) 109–112.